


Astrocyte activation in the periaqueductal gray promotes descending facilitation to cancer-induced bone pain through the JNK MAPK signaling pathway

Molecular Pain
Volume 15: 1–16
© The Author(s) 2019
Article reuse guidelines:
sagepub.com/journals-permissions
DOI: 10.1177/1744806919831909
journals.sagepub.com/home/mpx


Hua-dong Ni^{1,2}, Long Sheng Xu², Yungong Wang², Hongbo Li², Kang An³, Mingjuan Liu², Qianying Liu³, Houshen Deng², Qiuli He², Bing Huang², Jianqiao Fang¹, and Ming Yao² 

Abstract

Descending nociceptive modulation from the supraspinal structures has an important role in cancer-induced bone pain (CIBP). Midbrain ventrolateral periaqueductal gray (vlPAG) is a critical component of descending nociceptive circuits; nevertheless, its precise cellular and molecular mechanisms involved in descending facilitation remain elusive. Our previous study has shown that the activation of p38 MAPK in vlPAG microglia is essential for the neuropathic pain sensitization. However, the existence of potential connection between astrocytes and c-Jun N-terminal kinase (JNK) pathway in CIBP has not yet been elucidated. The following study examines the involvement of astrocyte activation and upregulation of p-JNK in vlPAG, using a CIBP rat model. Briefly, CIBP was mimicked by an intramedullary injection of Walker 256 mammary gland carcinoma cells into the animal tibia. A significant increase in expression levels of astrocytes in the vlPAG of CIBP rats was observed. Furthermore, stereotaxic microinjection of the astrocytic cytotoxin L- α -amino adipic acid decreased the mechanical allodynia as well as established and reversed the astrocyte activation in CIBP rats. A significant increase in expression levels of p-JNK in astrocytes in vlPAG of CIBP rats was also observed. Moreover, the intrathecal administration of JNK inhibitors SP600125 reduced the expression of glial fibrillary acidic protein, while microinjection of the SP600125 decreased the mechanical allodynia of CIBP rats. These results suggested that CIBP is associated with astrocyte activation in the vlPAG that probably participates in driving descending pain facilitation through the JNK MAPK signaling pathway. To sum up, these findings reveal a novel site of astrocytes modulation of CIBP.

Keywords

Cancer-induced bone pain, hyperalgesia, c-Jun N-terminal kinase, periaqueductal gray, descending facilitation, astrocyte

Introduction

Cancer-induced bone pain (CIBP) is one of the most common symptoms observed in patients with primary and metastatic bone cancer which significantly impacts the patients' quality of life.^{1,2} Clinically, CIBP mechanisms are complex and may involve a combination of inflammatory responses and neuropathic pain.³ Nevertheless, the specific cellular and molecular mechanisms underlying CIBP remain unclear. Accordingly, there is an urgent need to explore new targets for the therapeutic intervention.

Preclinical studies have demonstrated that hyperalgesia and allodynia are associated with the activation of

descending modulatory circuits involving descending facilitation.^{4–6} These pathways include the activation of descending pain nociceptive systems from the

¹The Second Clinical Medical College, Zhejiang Chinese Medicine University, Hangzhou, China

²Department of Anesthesiology and Pain Research Center, The First Affiliated Hospital of Jiaxing University, Jiaxing, China

³Department of Anesthesiology, Bengbu Medical College, Bengbu, China

Corresponding Author:

Ming Yao, Department of Anesthesiology and Pain Research Center, The First Affiliated Hospital of Jiaxing University, Jiaxing 314001, China. Email: jxyaoming666@163.com



periaqueductal gray (PAG)⁷ and rostral ventromedial medulla (RVM).^{8,9} The ventrolateral portion of the PAG (vlPAG) is a core component of the descending nociceptive system which projects to the RVM.^{10–14} Although numerous studies have shown that vlPAG has an important role in descending pain^{15,16,17–19} the precise underlying cellular and molecular mechanisms involved in descending facilitation remain elusive and need to be further investigated.

Recent progress in research on pain has indicated that glial cells such as microglia and astrocytes at supraspinal sites become reactive in chronic pain conditions and in turn contribute to the activation of descending modulatory circuits.^{7–9} Accumulating evidence demonstrates that the activation of JNK, a member of the mitogen-activated protein kinases (MAPK) family, induces the production of proinflammatory cytokines in spinal astrocytes after peripheral inflammation, nerve injury, or CIBP.^{20–22} In our previous studies,⁷ we have confirmed a contribution of astrocyte activation in the vlPAG that participates in driving descending pain facilitation of neuropathic pain. Due to considerable mechanistic differences between nerve injury and CIBP, we investigated whether CIBP by intramedullary injection of Walker 256 mammary gland carcinoma cells into the tibia is capable of causing astrocyte activation in the vlPAG, and to determine whether this astrocyte activation contributes to descending facilitation.

Materials and methods

Animals

Female adult Sprague-Dawley (SD) rats, eight weeks old, weighing 190–220 g were obtained from Experimental Animal Center of Zhejiang Chinese Medicine University, China. All the animals were raised in plastic cages (five rats in one cage) and housed in an environment with temperature of $22 \pm 1^\circ\text{C}$, relative humidity of $50 \pm 1\%$ and a light/dark cycle of 12/12 h. Animals had access to food and water ad libitum. In addition, all animal studies (including the rat euthanasia procedure) were done in compliance with the regulations and guidelines of Zhejiang Chinese Medicine University institutional animal care and were conducted according to the National Institutes of Health Guide for the Care and Use of Laboratory Animals and the IASP guidelines for pain research. Best efforts were exerted to minimize the amount of animals use and their suffering.

The experimental protocol was divided into six parts:

1. Bone cancer pain model was established and validated. Rats were randomly divided into CIBP and sham (injection heat-killed Walker 256 cell) group ($n = 10/$

group). Paw withdrawal threshold (PWT) of the ipsilateral hind paw was observed one day before and 6, 12, and 18 days post-surgery. Next, additional 20 rats were randomly divided into five groups ($n = 4/\text{group}$): naïve, sham, 6, 12, and 18 days post-surgery group. The bone cancer pain model was examined by radiography and immunohistochemistry.

2. It was determined whether the astrocytes and JNK MAPK activation occurred in the vlPAG of CIBP-treated rats. Briefly, 56 rats were randomly divided into seven groups ($n = 8/\text{group}$): naïve, CIBP (6, 12, 18 d) and sham (6, 12, 18 d) groups. After each time point, rats were anesthetized and then perfused with fixative. The tissue samples were analyzed using immunohistochemistry ($n = 4$) or Western blot/real time polymerase chain reaction (RT-PCR) ($n = 4$).
3. It was determined whether the astrocytes activation contributes to the development of enhanced pain after tumor cell inoculation. Rats were randomly divided into four groups: Sham+Veh ($n = 18$), CIBP+Veh ($n = 18$), CIBP+LAA 100 ($n = 18$), and CIBP+LAA 1 ($n = 10$) groups. Twelve days after tumor cell inoculation, the rats received a continuous vlPAG microinjection of either saline (Veh) or LAA 100 nmol. In a separate group, 6 days after injection of LAA or Veh, rats were anesthetized and then perfused with fixative. The tissue samples were analyzed using immunohistochemistry ($n = 4$) or Western blot/RT-PCR ($n = 4$).
4. It was determined whether p-JNK MAPK is present in vlPAG glial cells and neurons. Tissue sections from day-12 surgery animals were labeled with fluorescent marker for p-JNK MAPK and colabeled with OX-42 (microglial marker), glial fibrillary acidic protein (GFAP; astrocytic marker), or NeuN (neurological marker).
5. A specific role of PAG JNK in the maintenance of bone cancer pain was examined. Briefly, a JNK inhibitor (SP600125) was microinjected once a day, at three different dosages. Rats were randomly divided into six groups: Sham+Veh ($n = 14$), CIBP+Veh ($n = 14$), CIBP+SP 50 ($n = 14$), CIBP+SP 10 ($n = 10$), CIBP+SP 2 ($n = 10$), and Sham+SP 50 ($n = 10$) groups. Twelve days after cell inoculation, rats received a continuous vlPAG microinjection of either saline+5%DMSO (Veh) or SP (50, 10, and 2 nmol) ($n = 10$). In a separate group, 4 days after injection of SP or Veh, rats were anesthetized and then perfused with fixative. Tissue samples were analyzed using Western blot ($n = 4$).
6. Examine the association between tumor cell inoculation-induced astrocytes activation and JNK MAPK phosphorylation within the vlPAG. Rats were randomly divided into three groups ($n = 8/\text{group}$). From day 12 post-surgery, a specific p-JNK MAPK inhibitor SP (or Veh) was injected into the

vIPAG of CIBP rats. On day 16, CIBP rats were euthanized and their tissues were further analyzed using GFAP Western blot ($n = 4$) and immunohistochemistry ($n = 4$).

Preparation of cells

The Walker 256 mammary gland carcinoma cells (Institute for Biomedical Research of Shanghai, China) were cultured in RPMI-1640 medium containing 10% fetal bovine serum, streptomycin (100 U/ml), and penicillin (100 U/ml) in a humidified atmosphere containing 5% CO₂/95% air at 37°C.

Cells were washed three times in 0.1 M sodium phosphate buffer saline (PBS) and resuspended in 1 ml at a density of 2×10^7 cells/ml. Cells were then injected into the abdominal cavities of young female SD rats (weighing 60–80 g). The cancerous ascites developed after 6–7 days. The ascites were washed with sterilized PBS by centrifugation in 10 ml of medium for 3 min at 2000 r/min for three times. The resulting pellet was resuspended in PBS and then diluted to a final concentration of 1×10^5 cells/10 μ l. The cell suspension was kept on the ice until injection.

Bone cancer model

Injection protocol of Walker 256 mammary gland carcinoma cell was performed as previously described (see “Preparation of cells” section). Briefly, rats were subjected to anesthesia using chloral hydrate (300 mg/kg, i.p.). Then, a superficial incision was made to expose the tibial plateau. A 30-gauge needle was inserted into the bone cortex, and a light depression was made using a 50- μ l microinjection. Consequently, 1×10^7 cells (10 μ l) heat-killed Walker 256 cell or 1×10^7 cells (10 μ l) Walker 256 cells were injected into the medullary cavity of the tibia, corresponding to control rats or tumor-bearing rats. Afterward, the injection site was sealed with a medical glue followed by copious irrigation with sterile saline. The wound was then closed by medical glue.

Assessing the extent of bone destruction

Radiology. The rats were radiographed at 6, 12, and 18 days after inoculation to verify cancer development in the tibia. After the rats were anesthetized with pentobarbital sodium (50 mg/kg, i.p.), the hind limbs were placed on X-ray film (Kodak, Italy) and exposed to X-ray for 1/20 s at 40 kVp. The images were taken from sham rats and CIBP rats.

Histochemical staining. Rats tibia were embedded in paraffin after demineralizing in EDTA (10%) for 2–3 weeks; 10- μ m sections were cut and stained with Harris’

hematoxylin and eosin to verify malignant cell infiltration and bone destruction.

Behavioral testing

The general health of the animals was evaluated daily. The body weight was measured at 0, 6, 12, and 18 days post-injection, in both sham rats and CIBP rats. Animals were familiarized with the testing environment daily for at least two days before baseline testing. Then, the rats were placed on a wire-mesh floor covered with a plexiglass chamber (20 \times 10 \times 10 cm) and allowed at least 30 min for habituation. A set of VonFrey monofilaments (BME-404, Institute of Biological Medicine, Academy of Medical Science, China) was used to test the mechanical PWTs as previously described. The monofilaments were held against the plantar surface of the hind paw until the rats withdrew the paw or licked the feet. After five consecutive tests at 10-s intervals, the values were averaged to yield a PWT. PWT was measured prior to surgery and on days 6, 12, or 18 post-surgery, as well as at various time points after microinjection.

vIPAG cannulation

Rats were anesthetized with 2% to 3.5% isoflurane using a gas mixture of 25% O₂ balanced with nitrogen and were placed in a stereotaxic apparatus (RWD Life Science Co., China) according to our previous reports. After infiltration of lidocaine (2%) into the scalp, a 1.5-cm midline incision was made. The underlying tissue was retracted with hemostats to expose the skull. A 7-mm stainless steel guide cannula (23-gauge) was implanted into the unilateral vIPAG (7.6 mm posterior to bregma, 0.6 mm lateral from the midline, and 5.8 mm beneath the surface of the skull).²³ A dummy cannula (28-gauge stainless steel wire) was inserted into the guide cannula to reduce the incidence of infection and clogging. Rats were given at least five days to recover before experimentation. Drugs (0.5 μ l) were administered through a 28-gauge injection cannula extending 0.5 mm beyond the tip of the guide cannula. The injection cannula remained in place for an additional 2 min to prevent the backflow of the drug after completion of drug infusion. The microinjection of drug was administered at 8 a.m. daily, which was 30 min before the behavioral test. At the termination of the experiments, cannulation sites in the vIPAG were verified histologically for proper placement; only data from rats with correctly placed injections were included in the analysis (Figure 1). Animals were then subjected to intra-vIPAG microinjection with the following inhibitors: L- α -amino adipic acid (LAA 100 nmol or 1 nmol, Sigma, USA) was dissolved in 1 M HCl and then diluted in sterile 0.9% saline; the JNK inhibitor SP600125 (2, 10, and 50 nmol, Sigma, USA)

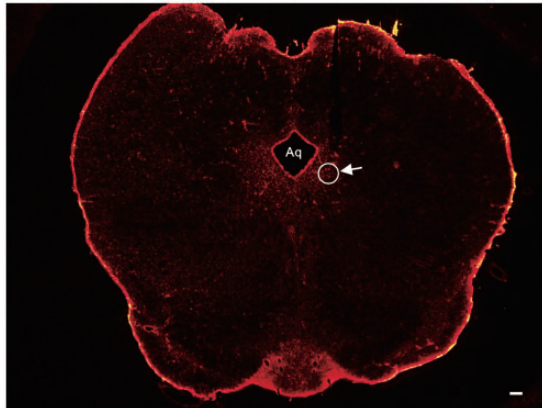


Figure 1. A representative photomicrograph of a coronal slice (vIPAG) stained with red fluorescent stain. The arrow indicates the tip position of the cannulation sites and the circle shows the site of injection. Scale bars = 100 μ m. Aq: aqueduct.

was dissolved in 5% dimethyl sulphoxide (DMSO) and then diluted with 0.9% saline. The vehicle group rats underwent identical procedures with injection of 0.5 μ l 5% DMSO in sterile 0.9% saline. Doses employed were selected according to the results of our pilot studies.

Immunohistochemistry

Under deep anesthesia with chloral hydrate (500 mg/kg, intraperitoneally), the rats were transcardially perfused with 250 ml of saline (0.9% NaCl) followed by 300 ml cold (4°C) 0.1 M phosphate buffer (PB, PH 7.4) containing 4% paraformaldehyde. The brain tissue between -6.96 and -8.52 mm caudal to bregma²³ which contained the PAG was then removed, post-fixed in the same fixative for 4–6 h at 4°C, then immersed in cryoprotective 30% sucrose in PB for 24–48 h at 4°C. PAG coronal sections were cut with the vibratome to a thickness of 30 μ m. All the sections were blocked with 5% donkey serum at room temperature (RT) for 1 h, then incubated at 4°C overnight with one of the following primary antibodies: rabbit anti-GFAP (1:1500 dilution, Abcam), rabbit anti-Iba-1 (1:300, Wako), or mouse anti-phospho-JNK MAPK (1:1000, Cell Signaling Technology). Following three, 10-min rinses in 0.1 M PBS, the sections were incubated with Cy3-conjugated donkey anti-rabbit secondary antibody solution (1:400, Jackson immunolab) or donkey anti-mouse secondary antibody solution (1:400, Abcam) at RT for 1 h, then washed with PBS. For double immunofluorescence staining, PAG sections were incubated overnight at 4°C with a mixture of the following antibodies: Mouse anti-p-JNK and rabbit anti-Iba-1 (1:300, Wako), Mouse anti-p-JNK and rabbit anti-GFAP (1:1500, Abcam), and Mouse anti-p-JNK and rabbit anti-NeuN (1:200,

Millipore). This was followed by 1.5 h incubation at RT with a mixture of Cy3-conjugated donkey anti-mouse antibody and FITC donkey anti-rabbit antibody (1:200, Santa Cruz). All sections were cover slipped with 30% glycerin in 0.01 M PBS, then examined with a Nikon Confocal fluorescence microscope. The stained sections were analyzed by Image Pro-plus 6.0 (Image Pro-Plus Kodak, USA) and images were captured with a CCD Spot camera. The specificity of immunostaining was verified in the absence of primary antibodies.

Western blot analysis

Following anesthesia with isoflurane, rats were sacrificed by decapitation. Then, 2-mm thick coronal slice of the mesencephalon between -6.96 and -8.52 mm caudal to bregma was collected. Radial segments corresponding to the ipsilateral vIPAG were dissected under a stereomicroscope with the boundaries that were defined following anatomical criteria.²⁴ The vIPAG tissue was harvested, immediately frozen in liquid nitrogen, and stored at -80°C. Samples were then homogenized in lysis buffer containing 150 mM NaCl, 20 mM Tris-HCl (PH 7.6), 1 mM EDTA, 1% NP-40, 1 mM phenylmethanesulfonyl fluoride, protease inhibitor cocktail (Sigma, St. Louis, MO), and phosphatase inhibitor cocktail (Sigma). The lysates were centrifuged at 15,000 r/min for 15 min at 4°C, and the supernatant was then removed. Protein concentration was determined using a bicinchoninic acid assay (Pierce, Rockford, IL). Each sample containing 30 μ g of protein was separated on a 10% sodium dodecyl sulfate polyacrylamide gel electrophoresis and blotted on to a nitrocellulose membrane (Bio-Rad). The membranes were blocked with 5% nonfat dry milk in tris-buffered saline containing 0.1% Tween-20 for 3 h at RT. The following primary antibodies were used to probe the blots: Mouse anti-JNK (1:4000, Cell Signaling Technology), Mouse anti-p-JNK (1:4000, Cell Signaling Technology), and rabbit anti-GFAP (1:2500, Abcam), respectively. For loading control, the blots were incubated with GAPDH antibody (1:20000, mouse, Sigma). All the blots were incubated overnight at 4°C with primary antibody. Bound primary antibodies were detected following incubation at RT for 1 h with the appropriate horseradish peroxidase-conjugated anti-rabbit or anti-mouse secondary antibody (1:10000, Jackson immunolab). Immunoreactive (IR) bands were detected by using enhanced chemiluminescence (Thermo Scientific) and exposed to X-ray films. GAPDH served as a loading control monitor.

Real-time polymerase chain reaction

Total RNA was extracted from vIPAG (the method of dissection is consistent with WB experiment mentioned

above) with the Trizol reagent (Invitrogen, Carlsbad, CA). One microgram of total RNA was converted into cDNA using PrimeScript RT reagent kit (Takara, Otsu, Shiga, Japan). The cDNA was amplified using the following primers: GFAP forward 5'- AGA AAA CCG CAT CAC CAT TC -3', reverse 5'- GCA CAC CTC ACA TCA CAT CC -3'; p-JNK forward 5'- CGG AAC ACC TTG TCC TGA AT -3', reverse 5'- GAG TCA GCT GGG AAA AGC AC -3'; and GAPDH forward 5'- TCT CTG CTC CTC CCT GTT C -3', reverse 5'- ACA CCG ACC TTC ACC ATC T -3'. The PCR was performed using a 2720 thermal cycler (Applied Biosystems). The SYBR Premix Ex Taq II kit (Takara) was used for all PCR reactions. The PCR reactions were run on a Rotor-Gene 6000 RT-PCR machine (Corbett Research, Mortlake, Australia). The melting curves were performed to validate the utility and specificity of each PCR product. The data were analyzed using Rotor-Gene 6000 series software and evaluated using the comparative CT Method ($2^{-\Delta\Delta CT}$).

Statistical analysis

SPSS version 20.0 was used to determine the statistical significance. Results were expressed as mean \pm standard deviation. When only two groups were compared, Student's *t* test was used. Differences between groups were compared using one-way analysis of variance (ANOVA) or two-way repeated measures ANOVA followed by Bonferroni's. $P < 0.05$ was considered statistically significant.

Results

Radiological, behavioral, and histochemical analysis of tumor development in rat tibia

Tibia destruction by tumor was examined by radiography. No structural destruction was observed in naïve group and sham group (Figure 2(a) and (b)). In contrast, radiological analysis revealed minute bone trabecula

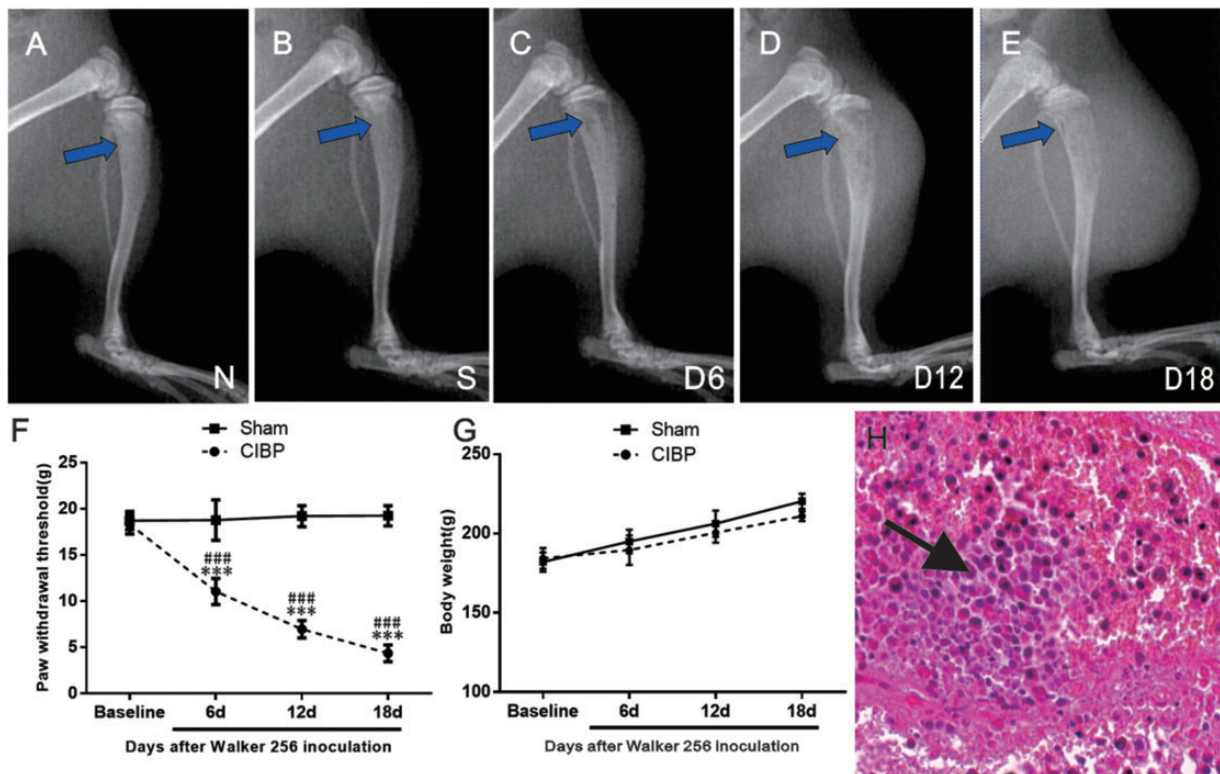


Figure 2. Radiological, behavioral, and histochemical analysis of tumor development in the right tibia. On day 18 after inoculation, intact bone was observed in both naïve group (a) and sham-operated rats (b); while mild (c) and evident (c and d) bone destruction were observed in the CIBP group on 6th, 12th, and 18th day post-surgery, respectively. (f) The ipsilateral PWT progressively decreased from day 6 to day 18 in CIBP rats. Sham group rats showed no significant change in pain sensitivity. Data were expressed as mean \pm SEM. $n = 10$ rats in each group (** $P < 0.001$; vs. Baseline, #### $P < 0.001$; vs. Sham group). (g) The body weight was gradually increased in both sham rats and BCP rats during an 18-day observation period. (h) Hematoxylin and eosin staining of the right tibia showed that bone marrow spaces were infiltrated with malignant tumor (see the arrow) on day 18 after Walker 256 cell inoculation. CIBP: cancer-induced bone pain.

defects in the proximal epiphysis six days after tumor cell inoculation (Figure 2(c)). Further deterioration was detected at 12 days post-surgery with full thickness unicortical bone loss (Figure 2(d)). In addition, full-thickness, bicortical, bone loss, as well as cortical destruction and soft tissue tumors were observed at day 18 after cell injection (Figure 2(e)).

All rat groups exhibited similar baseline hind PWT to mechanical stimulation (vonFrey filaments) ($P > .05$; vs. Sham group; ANOVA; $n = 10$; Figure 2(f)). PWT of the ipsilateral hind paw progressively decreased compared with sham rats on day 6 of CIBP ($F_{3, 54} = 192.6$, $***P < 0.001$; vs. Baseline; two-way repeated measures ANOVA; $n = 10$; Figure 2(f)). With the progression of bone cancer, a significant decrease in PWT of the ipsilateral hind paw was observed in CIBP rats compared with sham rats between 6 and 18 days post-surgery ($F_{1,18} = 471.6$, $####P < 0.001$; vs. sham group; two-way repeated measures ANOVA; $n = 10$; Figure 2(f)). These results suggested the development of mechanical allodynia in the inoculated hind paw.

In addition, during the 18-day observational period, all rats showed general good health and mild increase in body weight in both sham group and CIBP group (Figure 2(g)). On day 18 after tumor cell inoculation, a malignant tumor infiltration in the bone marrow spaces was observed by histological analysis (Figure 2(h)), while bone destruction was not observed in the sham or vehicle group animals (data not shown).

Increase of vIPAG GFAP expression in CIBP rats

Astrocytes are the most abundant cells in the CNS. Our previous studies have demonstrated that astrocyte activation contributes to descending facilitation of neuropathic pain.⁷ To examine whether the astrocyte expression in vIPAG, immunofluorescence labeling was used to detect GFAP in naive, sham-operated, and tumor inoculated rats. In naive and sham-operated rats, astrocytes appeared to be in a resting state showing even spacing at vIPAG sections (Figure 3(b) and (c)). Compared to naive and sham groups, vIPAG sections exhibited increased GFAP immunostaining along with morphological changes that were hypertrophic with thick, more processes and increased density of GFAP staining (Figure 3(d) to (f)). The expression of GFAP progressively increased, by reaching the maximum levels on day 18 following Walker 256 cells inoculation (Figure 3(d) to (f)).

The findings were additionally confirmed by Western blot and RT-PCR. Western blot analysis showed a significant expression of PAG astrocyte protein on days 6–18 ($F_{6,21} = 171.2$, $***P < 0.001$; vs. Naive group; one-way ANOVA; $n = 4$; Figure 3(g)), while no changes were observed in naive and sham animals

($P > 0.05$; vs. Naive group; ANOVA; $n = 4$; Figure 3(g)). In addition, RT-PCR and the number of GFAP IR cells revealed a parallel and significant increase in PAG GFAP mRNA at 6, 12, and 18 days in CIBP animals ($F_{4, 15} = 56.61$, $***P < 0.001$; vs. Naive group; one-way ANOVA; $n = 4$; Figure 3(h); $F_{4, 15} = 77.15$, $***P < 0.001$; vs. Naive group; one-way ANOVA; $n = 4$; Figure 3(i)).

Tumor-induced hypersensitivity and GFAP expression is reversed by astrocyte cytotoxin

To determine whether astrocyte hyperactivation in the vIPAG could ameliorate the CIBP, 0.5 μ l astrocytic cytotoxin L- α -amino adipate (LAA 100 nmol or 1 nmol) was microinjected into the vIPAG once per day for a total of seven days. On the 12th day post-surgery, CIBP rats showed mechanical allodynia represented by significant reductions in paw withdrawal threshold. The injection of LAA (100 nmol) into the vIPAG of naive rats did not produce detectable behavioral changes relative to the baseline values (data not shown). Compared with CIBP + veh group, micro-administration of LAA significantly elevated the PWTs of the CIBP rats in a dose-dependent manner ($F_{3,36} = 1758$, $***P < 0.001$ vs. CIBP+Veh group; $####P < 0.001$, $##P < 0.01$ vs. CIBP+LAA 1 nmol group; two-way ANOVA; $n = 10$; Figure 4(d)), which effect started at postoperative day (POD) 14, two days after the beginning of LAA treatment. The analgesic effect of LAA (100 nmol) was still observed at POD 20, two days after the treatment was stopped. Yet, the effect of LAA (1 nmol) at lower dosages lasted only for 24 h after drug withdrawal.

To identify whether the analgesic effect of LAA (100 nmol) was mediated by its influence on the astrocytes in vIPAG, we further examined the expression of GFAP (astrocyte marker) on POD 18 in various groups (Figure 4(a) to (c)). Based on the immunofluorescent staining analysis, the GFAP immunoreactivity was barely observed in Sham rats receiving vehicle (Figure 4(a)), while a significant increase in GFAP positive cells was observed in the rats receiving vehicle following tumor cell inoculation (Figure 4(b)). Intra-vIPAG microinjection of LAA reduced the number of GFAP positive cell ($F_{2,9} = 57.41$, $***P < 0.001$; vs. Sham+Veh; $####P < 0.001$; vs. CIBP+Veh; one-way ANOVA; $n = 4$; Figure 4(c) and (f)). The immunofluorescence data were further confirmed in Western blot analysis ($F_{2,9} = 58.39$, $***P < 0.001$; vs. Sham+Veh; $####P < 0.001$; vs. CIBP+Veh; one-way ANOVA; $n = 4$; Figure 4(e)). All these results suggested that vIPAG astrocyte activation has an important role in maintaining the hypersensitivity in CIBP.

At the same time, we examined the effect of LAA on microglial function on POD 18 in the vIPAG in CIBP

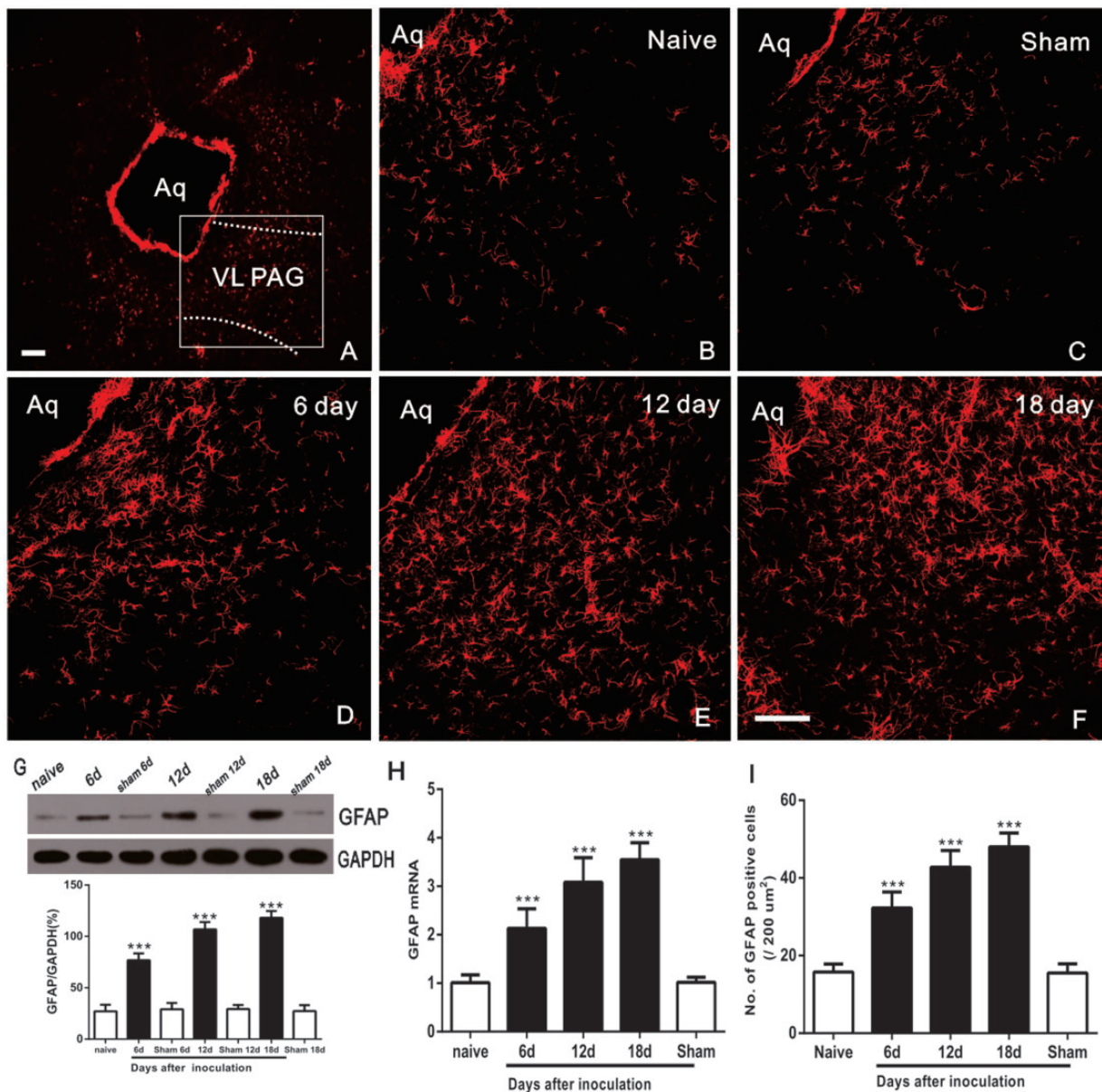


Figure 3. Time-course-dependent hyperactivation of astrocytes in the VL-PAG after inoculation. (a) Low-power view of the PAG. The dotted lines show the location of the VL-PAG. The rectangle represents the location of photomicrographs (b to f) showing GFAP immunostaining in the VL-PAG of naive rats, sham rats, and at 6, 12, and 18 days after inoculation. (g) Western blot analysis of changes in GFAP protein levels over time in the VL-PAG (***) $P < 0.001$ vs. naive group; $n = 4$). (h and i) RT-PCR and the number of GFAP immunoreactive cells revealed a parallel and significant increase in PAG at 6, 12, and 18 days in CIBP model (***) $P < 0.001$ vs. naive group, $n = 4$). Scale bars = 100 μm . Aq: aqueduct; VL-PAG: ventrolateral periaqueductal gray; GFAP: glial fibrillary acidic protein; GAPDH: glyceraldehyde 3-phosphate dehydrogenase.

model. The Iba1 immunoreactivity was barely observed in Sham rats receiving vehicle (Figure 4(g)), while a significant increase in Iba1 positive cells was observed in the rats receiving vehicle on POD 18 (Figure 4(h)). In addition, the intra-vIPAG microinjection of LAA did not block tumor cell inoculation-induced enhancement of Iba1 expression ($F_{2,9} = 80.16$, ***) $P < 0.001$; vs. Sham+Veh; one-way ANOVA; $n = 4$; Figure 4(i) and (k)).

The immunofluorescence data were further confirmed by Western blot ($F_{2,9} = 44.42$, ***) $P < 0.001$; vs. Sham+Veh; one-way ANOVA; $n = 4$; Figure 4(j)).

Tumor cell inoculation induces significant upregulation of astrocytic pJNK in vPAG

To explore the role of pJNK in CIBP, we examined the JNK activation in vIPAG at different time points after

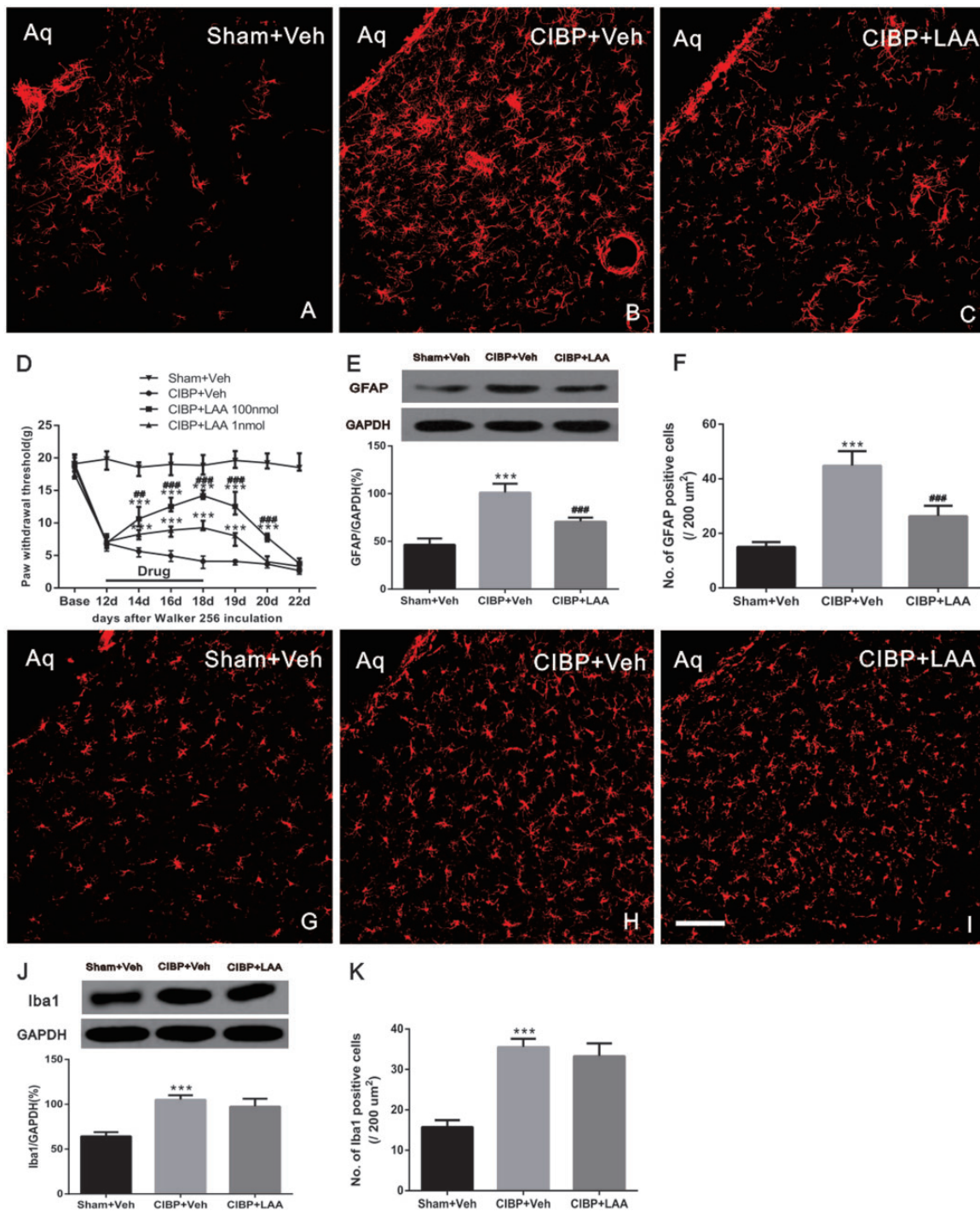


Figure 4. Tumor cell inoculation-induced hypersensitivity and GFAP expression are reversed by astrocyte cytotoxin. Midbrain sections obtained from Sham rat injections of Veh (a) or CIBP and receiving microinjections of Veh (b) or 100 nmol of LAA (c) in the PAG were labeled with GFAP for immunofluorescent visualization of astrocytes. (d) LAA or Veh were administered once a day on POD 12 to 18. Compared with CIBP + veh group, microadministration of LAA significantly elevated the PWTs of the CIBP rats in a dose-dependent manner ($***P < 0.001$ vs. CIBP+Veh group; $####P < 0.001$, $###P < 0.01$ vs. CIBP+LAA 1 nmol group; $n = 10$). (e) PAG tissues were collected 1 h after the last injection. The WB shows continuous VL-PAG injection of LAA reversed the upregulation of GFAP in CIBP rats. GAPDH was used as a loading control ($***P < 0.001$ vs. Sham+Veh; $####P < 0.001$ vs. CIBP +Veh; $n = 4$ for each group). (f) The numbers of cells showing GFAP in each group is quantified ($***P < 0.001$ vs. Sham+Veh; $####P < 0.001$ vs. CIBP +Veh; $n = 4$ for each group $n = 4$). Midbrain sections obtained from Sham rat injected with Veh (g) or CIBP rats microinjected with Veh (h) or 100 nmol LAA (i) in the PAG were labeled with Iba1 for immunofluorescent visualization of microglia. (j and k) Intra-vPAG microinjection of LAA did not block tumor cell inoculation-induced enhancement of Iba1 expression. Scale bar: 100 μm. Aq: aqueduct; CIBP: cancer-induced bone pain; LAA; L-α-aminoadipic acid.

inoculation. Compared with naïve group (Figure 5(a)), tumor injection on day 12 resulted in a significant increase of pJNK immunoreactivity in vIPAG (Figure 5(c)); which was indicated by increased density of IR staining in high-magnification images (Figure 5(d)). In addition, there was no significant difference in pJNK expression in PAG between Sham Saline (Figure 5(b)) and naïve (Figure 5(a)) groups. These findings were confirmed by Western blot. The pJNK and JNK levels in vIPAG of CIBP rats on days 6, 12, and 18 were examined. It was found that tumor injection induced pJNK/JNK increase on days 12 and 18 after inoculation ($F_{6,21}=173.3$, $***P<0.001$; vs. naïve group; one-way ANOVA; $n=4$; Figure 5(e)), while no significant changes were observed on day 6 group, and naïve and sham rats ($P>0.05$; vs. Naive group; ANOVA; $n=4$; Figure 5(e)). pJNK activation was further measured with PT-PCR. pJNK mRNA persistently increased in vIPAG on days 12 and 18 in rats with tumor inoculation ($F_{4,15}=20.82$, $***P<0.001$; vs. naïve group; one-way ANOVA; $n=4$; Figure 5(f)), while no significant changes were found on day 6 in sham group ($P>0.05$; vs. Naive group; ANOVA; $n=4$; Figure 5(f)).

To detect the cellular localization of pJNK expression in vIPAG, double immunofluorescence staining with antibodies against pJNK and the microglial specific marker OX42, the neuronal marker NeuN, or the astrocytic specific marker GFAP were performed, respectively. Briefly, no colocalization was observed between pJNK and OX42 (Figure 6(a) to (c)) or between pJNK and NeuN (Figure 6(d) to (f)), which suggested that neither neurons nor microglia express pJNK in vIPAG 12 days after inoculation. However, all pJNK-positive cells were GFAP positive astrocytes (Figure 6(g) to (i)).

Inhibition of tumor-induced mechanical allodynia in the maintenance phase by JNK inhibitor

To confirm a specific role of vIPAG JNK in the maintenance of bone cancer pain, JNK inhibitor (SP600125) was microinjected once a day at different dosages; changes in PWT were observed 60 min after administration, from POD 13 to POD 16. Tumor cell inoculation induced significant mechanical allodynia as shown in the CIBP+Veh group (Veh is 5% DMSO+ normal saline). Compared to CIBP+Veh group, microinjection of 2 nmol/0.5 μ l SP600125 did not influence PWT ($P>0.05$ vs. CIBP+Veh group; two-way ANOVA; $n=10$; Figure 7(a)). Administration of 10 nmol/0.5 μ l and 50 nmol/0.5 μ l SP600125 elevated PWT significantly ($F_{5,54}=1104$, $***P<0.001$ vs. CIBP+Veh group; two-way ANOVA; $n=10$; Figure 7(a)). Furthermore, a higher dose of SP600125 (50 nmol/0.5 μ l) apparently elevated PWT ($F_{5,54}=1104$, $###P<0.001$ vs. CIBP+

SP 10 nmol/0.5 μ l group; two-way ANOVA; $n=10$; Figure 7(a)). Nevertheless, neither high (50 nmol/0.5 μ l) nor lower doses (10 and 2 nmol/0.5 μ l, data not shown) of SP600125 changed the basal threshold in the sham-operated group ($P>0.05$ vs. Sham+Veh group; two-way repeated measures ANOVA; $n=8$; Figure 7(a)). To sum up, these results demonstrate that the injection of SP600125 (50 and 10 nmol/0.5 μ l) produces an effective and reliable anti-allodynia effect in a dose-dependent manner on CIBP.

To determine whether the JNK pathway is inhibited by SP600125, the midbrain tissue was collected after behavioral testing (1 h after drug injection, at POD 16) and examined the phosphorylation of JNK. The level of pJNK protein showed a significant increase in CIBP rats treated with Veh compared with the sham rats treated with Veh ($F_{2,9}=120.2$, $***P<0.001$; vs. Sham+Veh group; one-way ANOVA; $n=4$; Figure 7(b)). After vIPAG microinjection of SP600125 (50 nmol/0.5 μ l) in CIBP rats, pJNK protein level was significantly lower compared with that in the CIBP rats that received the Veh injection ($F_{2,9}=120.2$, $###P<0.001$; vs. CIBP+Veh group; one-way ANOVA; $n=4$; Figure 7(b)). These results further indicated that JNK activation occurs within the vIPAG during tumor cell inoculation-induced mechanical allodynia.

Effects of microinjection SP600126 on tumor-induced astrocytic expression

To determine whether the activation of JNK in the vIPAG contributes to astrocyte activation, the effect of the specific pJNK inhibitor SP600125 on expression of GFAP in the vIPAG of CIBP rats was further analyzed. Drug or vehicle was microinjected once a day from POD 12 to POD 16. Immunohistochemistry data revealed that the expression of GFAP were significantly higher in CIBP rats treated with Veh compared to sham rats treated with Veh in vIPAG on day 16 ($F_{2,9}=99.8$, $***P<0.001$; vs. Sham+Veh group; one-way ANOVA; $n=4$; Figure 8(a), (b), and (e)). Following injection SP600125 on days 12, 13, 14, 15, and 16, there was a striking decrease in the number of GFAP IR cells in CIBP rats compared with BCP rats that received Veh on days 12, 13, 14, and 15 ($F_{2,9}=99.8$, $###P<0.01$; vs. CIBP+Veh group; one-way ANOVA; $n=4$; Figure 8(b), (c), and (e)).

The findings were further confirmed by Western blot. GFAP protein levels significantly increased in CIBP rats treated with Veh compared with those of Veh-treated sham rats ($F_{2,9}=166.3$, $***P<0.001$; vs. Sham+Veh group; one-way ANOVA; $n=4$; Figure 8(d)). In comparison with CIBP rats treated with Veh, microinjection of SP600125 into the vIPAG significantly decreased the protein levels of GFAP 16 days after inoculation

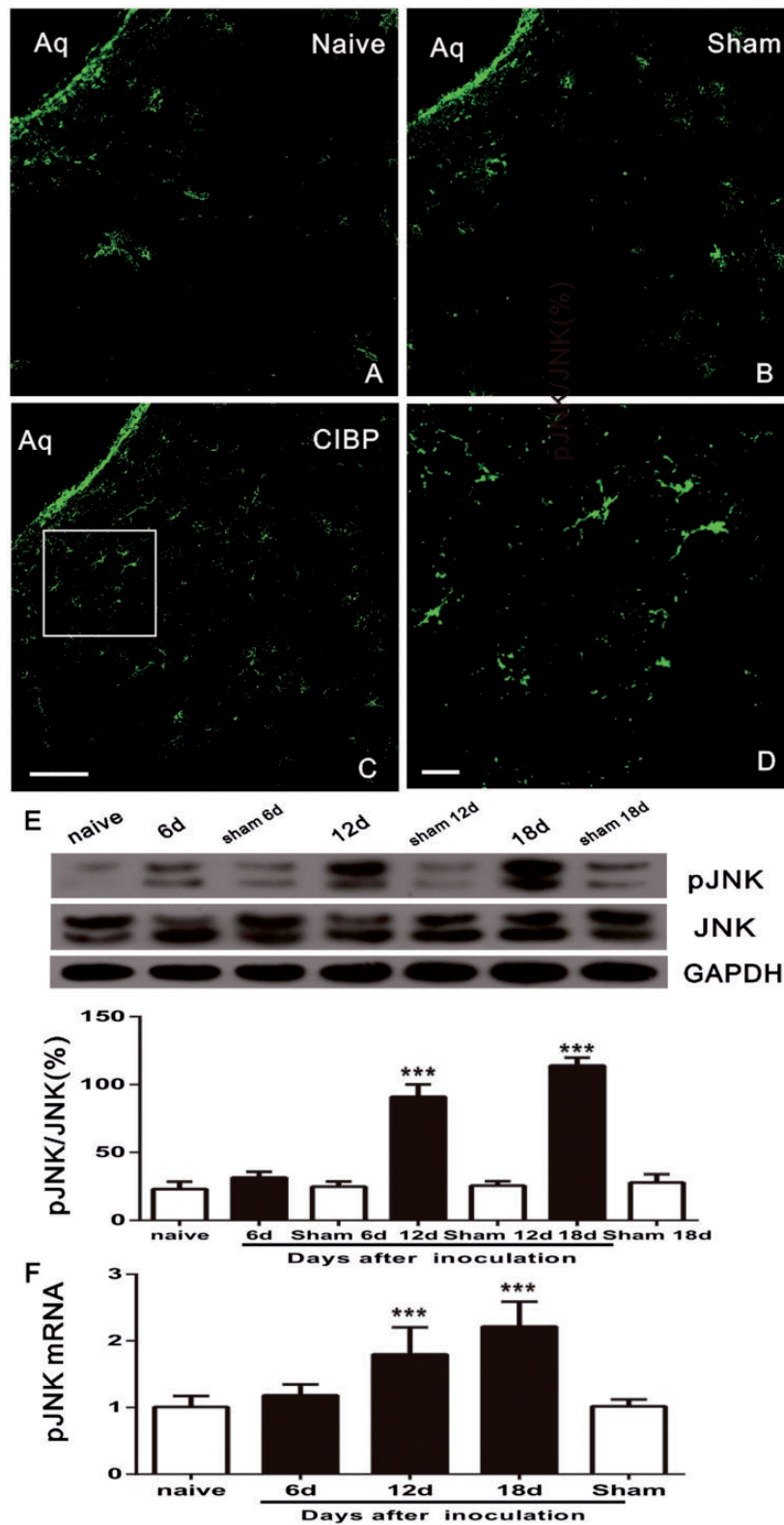


Figure 5. Tumor cell inoculation induces time-dependent activation of JNK in PAG. (a and b) Expression levels of pJNK in the PAG in naïve groups and Sham-Saline. (c) Upregulation of pJNK in PAG on postoperative day 12. (d) A high magnification image from the rectangle area of C shows a high density of pJNK-immunoreactive staining in PAG after inoculation. (e) Western blot results show an increase of pJNK/JNK in the PAG after tumor inoculation on days 12–18. pJNK expression gradually increased from day 12 to day 18; (***) $P < 0.001$; vs. naïve group; $n = 4$) (f) Real-time PCR revealed a persistent pJNK upregulation in PAG from day 12 to day 18; (***) indicates a statistically significant difference ($P < 0.001$) vs. naïve group. Four rats in each group. Scale bars: 100 μm in (c), (d), and (e), 20 μm in (d). Aq: aqueduct; CIBP: cancer-induced bone pain; JNK: c-Jun N-terminal kinase; GAPDH: glyceraldehyde 3-phosphate dehydrogenase; mRNA: messenger RNA.

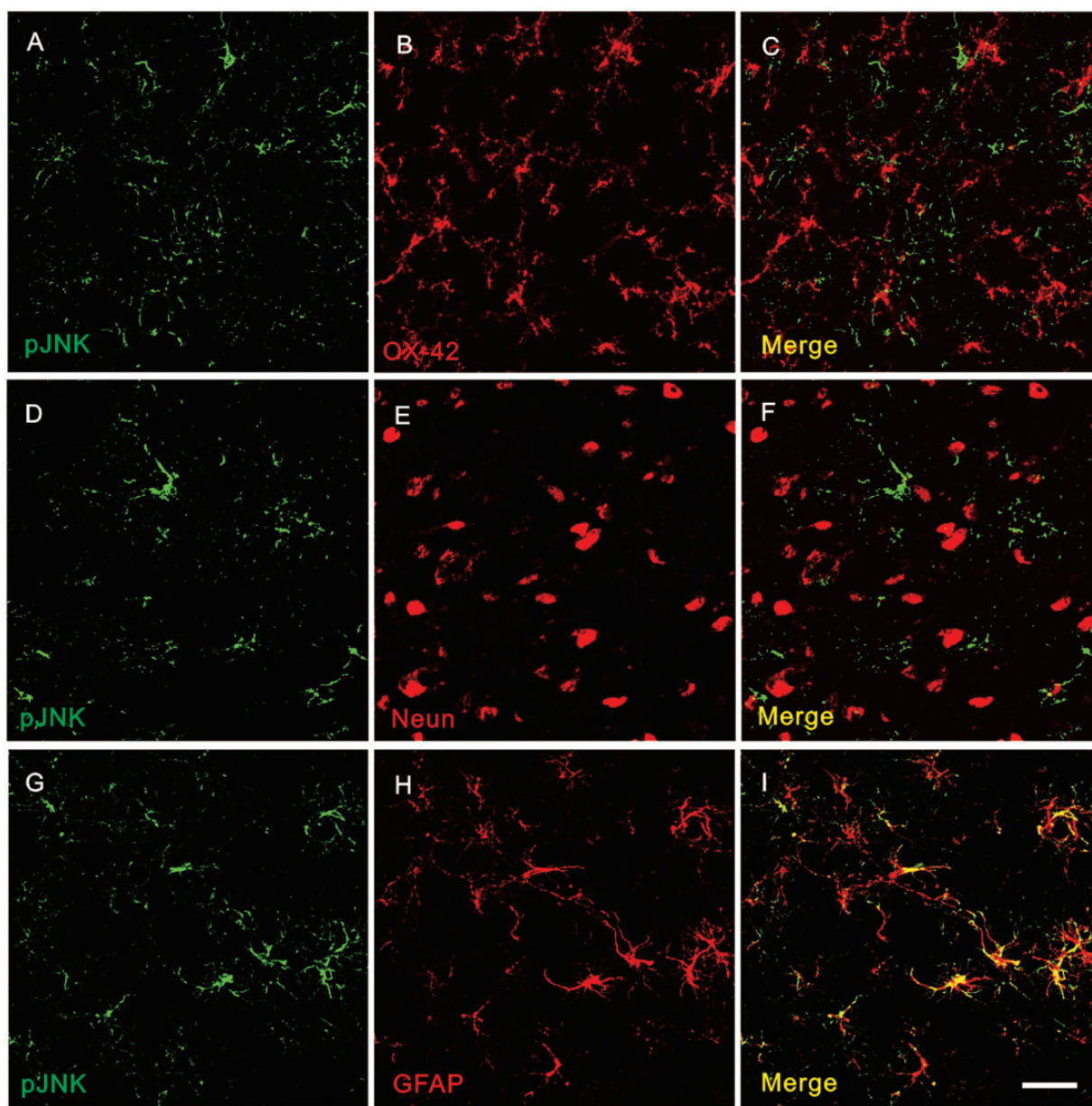


Figure 6. Cellular localization of pJNK expression in PAG after tumor cell inoculation. High-magnification images showing double immunofluorescent histochemical staining with OX-42 and pJNK (a to c), with NeuN and pJNK (d to f), or with GFAP and pJNK (g to i). Scale bar: 50 μ m.

Aq: aqueduct; GFAP: glial fibrillary acidic protein; JNK: c-Jun N-terminal kinase.

($F_{2,9} = 166.3$, $###P < 0.001$; vs. CIBP+Veh group; one-way ANOVA; $n = 4$; Figure 8(d)).

Discussion

Currently, the management of CIBP, which severely influences the quality of life in cancer patients, remains far from satisfactory.³ CIBP animal model, established by injecting Walker 256 cells into the tibia, has permitted scientists to elucidate the pathophysiological processes

through which cancer produces pain.²⁵ In the present study, we used the same model to demonstrate that CIBP regulates the activation of astrocytes in the vIPAG. Repetitive microinjection of the astrocyte cytotoxin L- α -aminoadipate into the vIPAG decreased behavioral signs of mechanical hyperalgesia/allodynia in a dose-dependent manner and inhibited the activation of astrocytes in the vIPAG. In addition, phosphorylation of JNK MAPK somewhat mediated the behavioral signs of CIBP, as repetitive microinjection of

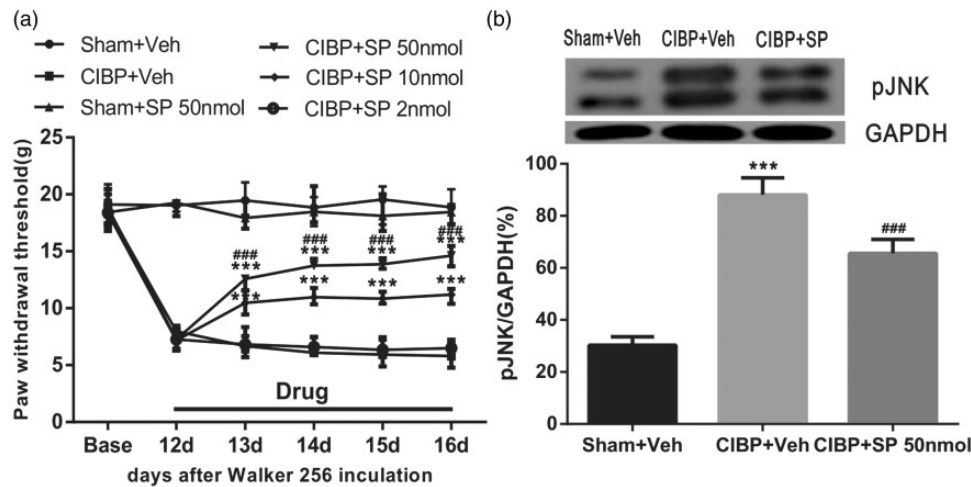


Figure 7. Effects of microinjection JNK inhibitor on tumor cell inoculation-induced mechanical allodynia. (a) Tumor cell inoculation induced significant mechanical allodynia as shown by von-Frey tests. Administration of 50 nmol/0.5 μ l SP600125 did not change the normal pain threshold of the sham operated group. Injection of (50 nmol/0.5 μ l, 10 nmol/0.5 μ l SP600125 showed an effective and reliable anti-allodynia effect in a dose-dependent manner on CIBP, whereas, injection of 2 nmol/0.5 μ l SP600125 did not influence pain threshold after inoculation at all. Drugs were given once a day from POD 12 to POD 16. *** P < 0.001, compared with that of CIBP+Veh group. #### P < 0.001, compared with that of CIBP+SP 10 nmol group. There were 10 rats in each group (SP600125:SP). (b) VL-PAG injection of SP600125 reversed upregulation of pJNK in CIBP. *** P < 0.001 vs. Sham+Veh, #### P < 0.001 vs. CIBP+Veh (n = 4 in each group). CIBP: cancer-induced bone pain; JNK: c-Jun N-terminal kinase; GAPDH: glyceraldehyde 3-phosphate dehydrogenase.

the JNK MAPK inhibitor SP600125 into the vlPAG decreased the mechanical allodynia. The activation of astrocyte JNK MAPK may be partly responsible for the behavioral expression of hyperesthesia due to CIBP, as the continuous microinjection of SP600125 into the vlPAG decreased GFAP labeling of vlPAG tissue. The results of the present investigation indicate that tumor cell inoculation induces astrocyte activation in the vlPAG, and that activated astrocyte JNK in vlPAG may contribute to enhanced pain, probably through the activation of descending facilitation from the PAG.

In past decades, converging lines of effort have been dedicated to investigating the endogenous pain modulating system.^{10,11,26,27} PAG, one of the core components of the descending pain modulatory system, has been proved to project to the RVM and the spinal cord.^{12,28} It is now acknowledged that the PAG, a central component of the descending system, is an integral part of pain signal inhibitory and facilitatory processing, particularly in chronic pain.¹³ Also, the vlPAG has shown to be an essential component of the neural substrate mediating pain modulation.^{4,5,14,19,29} Despite a growing number of evidence indicating a role vlPAG has in descending pain modulation, the precise underlying cellular and molecular mechanisms involved in descending modulation remain elusive.

Growing evidence has demonstrated that astrocyte cells in spinal cord contribute to the maintenance of inflammatory and neuropathic pain.³⁰⁻³⁵ Due to differences in animal species, sexes, and the origins of tumor

cells, there is a large variation in spinal astrocytic reaction in CIBP. Astrocytic activation has been frequently demonstrated in a vast majority of rat and mouse bone cancer pain models³⁶⁻³⁹ despite a recent report from Ducourneau et al.⁴⁰ which showed no increase in GFAP and S100 β in female SD rats injected with MRMT-1 cells. These studies have focused on their roles at the peripheral and spinal levels and on the activation of astrocyte cells in supraspinal structures. Attention in mounting number has been paid to the activation of astrocyte cells in supraspinal structures. For example, activated astrocytes were found in RVM after chronic constriction injury (CCI) of the rat infraorbital nerve,⁹ peripheral inflammation pain induced by carrageenan,⁸ bone cancer pain,⁴¹ and in PAG following CCI of the sciatic nerve.⁴²⁻⁴⁴

Our previous study⁷ has shown that astrocyte cells in the vlPAG are also involved in the neuropathic pain mediated descending pain facilitation. What's more, we attempted to reduce supraspinal astrocytic activation and to correlate such inhibition of astrocytic activation with changes in neuropathic pain. However, whether the activated astrocytes in vlPAG is involved in the development of bone cancer pain, which is an intricate symptom comprising the similar syndrome of inflammatory and neuropathic pain, remains unknown. It is also debated whether a sequent activation of spinal microglia and astrocytes occur in CIBP just like inflammatory and neuropathic pain. Unexpectedly, in the present study, we found that tumor cell inoculation may induce vlPAG

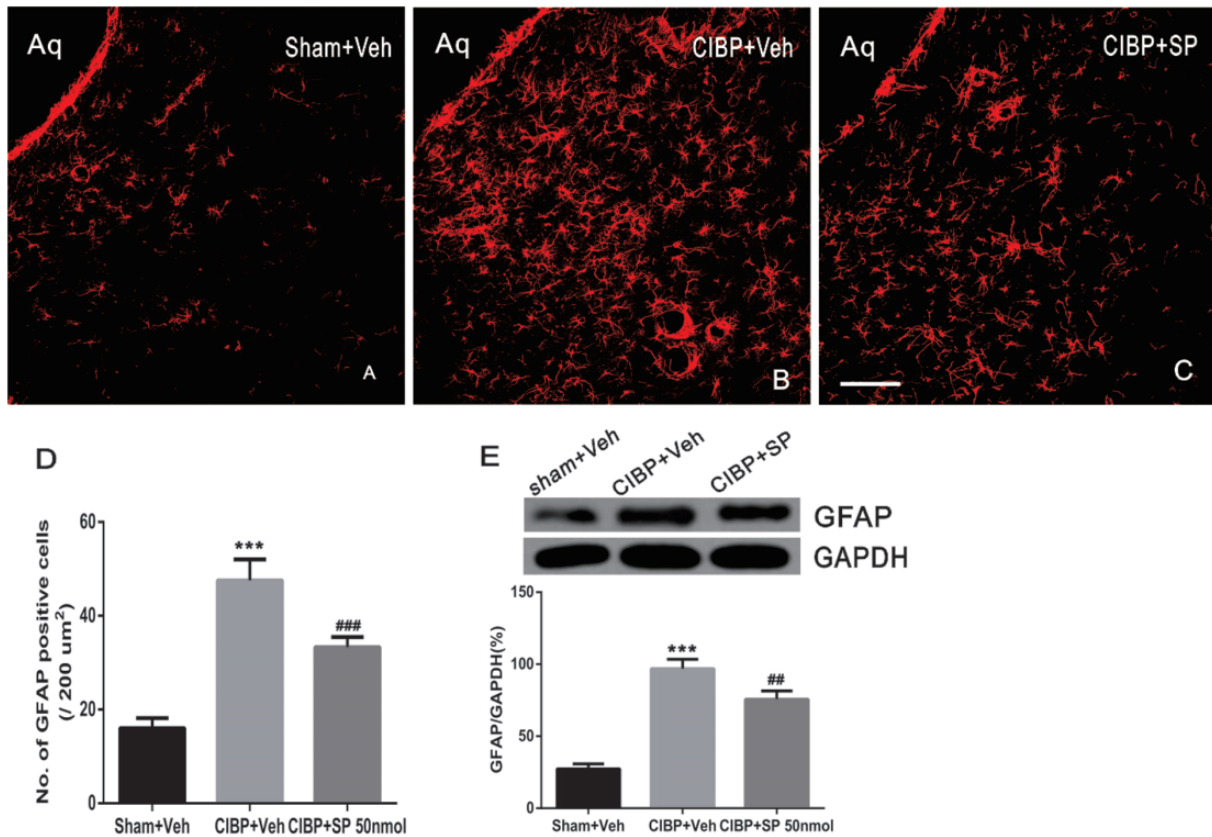


Figure 8. Suppression of GFAP expression by Intra-PAG JNK inhibitor. (a and b) There was a significant increase in the number of GFAP-IR cells in PAG of CIBP model rats treated with Veh (b) compared with sham rats treated with Veh (a) on day 16. (c) Intra-PAG JNK inhibitor provided a significant decrease of the GFAP positive cells in CIBP rats. (d and e) The number of GFAP immunoreactive cells and Western blot analysis following VL-PAG injection of SP600125 in CIBP rats ($n = 4$). *** $P < 0.001$ vs. sham+Veh group; #### $P < 0.001$, ### $P < 0.01$ vs. CIBP+Veh group. Scale bar = 100 μm .

CIBP: cancer-induced bone pain; Aq: aqueduct; GFAP: glial fibrillary acidic protein; GAPDH: glyceraldehyde 3-phosphate dehydrogenase.

astroglial activation after six days. These data were further verified by Western blot and RT-PCR analysis, which showed elevated expression of GFAP proteins and mRNA on days 6–18 after cell inoculation. These results suggested that astrocyte in the vlPAG have an important role in induction and maintenance of CIBP. Furthermore, our results are consistent with a previous research⁴⁵ that suggests that bone cancer induces rapid and persistent astrocytic activation in spinal cord on days 7–21. Continuous intra-vlPAG astrocyte cytotoxin reduced the development of bone cancer-induced allodynia and hyperalgesia and inhibited hyperactive astrocytes without microglial disruption in the vlPAG. This observation is also consistent with a recent study,⁹ which indicated that fluorocitrate, a selective inhibition of astrocytes, could be used to effectively inhibit the activation of astrocyte in CCI rats without apparent microglial disruption in the RVM. To sum up, the above data suggest that astrocyte activation in the vlPAG may promote descending facilitation to CIBP.

Among the multiple mechanisms of chronic pain, the role of MAPK activation including ERK, p38, JNK, and erk5 in central sensitization has been investigated over recent years. Evidence indicates that JNK activation occurs at different times in different animal models. For example, tumor cell inoculation may activate JNK in spinal cord after 12 days; and the levels remain elevated even after day 16 post-injection.⁴⁶ CFA induces persistent increase (1–28 days) of pJNK in both ipsilateral and contralateral spinal cord.²² Levels of p-JNK protein level in the ipsilateral spinal cord after SNL may increase after 10 injections.²¹ Although growing numbers of articles have indicated that spinal JNK activation is important in various pain conditions,^{31,47–51} comparatively little is known of its contribution to the vlPAG descending facilitatory system. Even though the mechanical thresholds in the present study were decreased on day 6 after tumor cell inoculation, the pJNK levels in vlPAG did not change compared to the naïve group at the early stage (<6 day).

This suggested that pJNK on day 6 might not be the relevant factor.

JNK has been found to be activated in spinal astrocytes but not in neurons or microglia after inflammatory and neuropathic pain.^{21,22,49} In our study, after intratibial inoculation with Walker 256 cells, increased levels of pJNK were found on day 12 only in the astrocytes but not in neurons and microglia in vIPAG. These findings suggest that the activation of astrocyte JNK MAPK may contribute to the development of CIBP through descending facilitation. Further investigations are necessary to explore this mechanism.

Several studies have also found that JNK1 in spinal astrocytes is required in inflammatory pain and neuropathic pain condition.^{22,52} According to our results, both pJNK1 and pJNK2 were increased in vIPAG on days 12–18, while continuous inhibition of JNK by SP600125 reduced the mechanical allodynia and astrocytic activation induced by CIBP surgery. These results further supported the concept that the activation of vIPAG astrocytes may be regulated by the JNK pathway and contribute to the development of CIBP, although the p-JNK signals triggering astrocytic activation in the vIPAG remain to be fully understood. In addition, the results from the behavioral tests revealed that there was no apparent influence of the intra-vIPAG of SP600125 on PWTs in the sham+SP group, indicating that the administration of SP did not affect the basal pain threshold.

In conclusion, the present study demonstrates that CIBP activates astrocytes as well as pJNK MAPK in astrocyte in the vIPAG. Microinjection of astrocyte cytotoxin or JNK MAPK inhibitors reduces tumor-induced mechanical allodynia. Western blot analysis showed that intra-vIPAG inhibitor injections also reverse or partially reverse astrocyte activation. Thus, vIPAG astrocyte activation appears to contribute to descending facilitation of CIBP development by activating the JNK MAPK signaling pathway. Additional studies are required to examine the effects of intracellular related receptors. Even though our findings contributed to solve a small part of this complex process, the precise descending pain modulatory system mechanisms require further research and confirmation.

Acknowledgments

The authors thank Renshan Ge (Wenzhou Medical University, China) for proofreading the paper.

Author Contributions

MY conceived and designed the study. HDN performed the experiments. HL, YW, and KA did the data analysis. BH, ML, and LSX coordinated and supervised the experiments. QL and YW participated in part of the behavioral testing and immunofluorescent staining experiments. HDN, QH, JF, and HN

wrote the article. All authors read and approved the final manuscript.

Availability of Data and Materials

All data generated or analyzed during this study are included in this published article.

Consent for Publication

Not applicable.

Declaration of Conflicting Interests

The author(s) declared no potential conflicts of interest with respect to the research, authorship, and/or publication of this article.

Ethics Approval

All animal procedures performed in this study were carried out in accordance with the guidelines of the International Association for the Study of Pain and were approved by the Zhejiang Chinese Medicine University Committee on Ethics in the Care and Use of Laboratory Animals.

Funding

The author(s) disclosed receipt of the following financial support for the research, authorship, and/or publication of this article: The study was supported by the National Natural Science Foundation of China (81341035), Natural Science Foundation of Zhejiang Province (LY16H090016, LQ19H090007), Medicine and Health Care General Studies Program of Zhejiang Province (2015KYA217), Zhejiang Provincial Program for the Cultivation of High-Level Innovative Health Talents (2012-RC-22), the Construction Project of Anesthesiology Discipline Special Disease Center in Zhejiang North Region (201524), and Jiaying City Science and Technology Project (2017AY33008, 2018AY32012).

ORCID iD

Ming Yao  <http://orcid.org/0000-0002-4226-8473>

References

1. van den Beuken-van Everdingen MHJ, de Rijke JM, Kessels AG, Schouten HC, van Kleef M and Patijn J. Prevalence of pain in patients with cancer: a systematic review of the past 40 years. *Ann Oncol* 2007; 18: 1437–1449.
2. Goblirsch MJ, Zwolak P and Clohisey DR. Advances in understanding bone cancer pain. *J Cell Biochem* 2005; 96: 682–688.
3. Falk S and Dickenson AH. Pain and nociception: mechanisms of cancer-induced bone pain. *JCO* 2014; 32: 1647–1654.
4. Dubovy P, Klusáková I, Hradilova-Svizenska I, Joukal M and Boadas-Vaello P. Activation of astrocytes and microglial cells and CCL2/CCR2 upregulation in the dorsolateral and ventrolateral nuclei of periaqueductal gray and

- rostral ventromedial medulla following different types of sciatic nerve injury. *Front Cell Neurosci* 2018; 12: 40.
5. Li Z, Yin P, Chen J, Jin S, Liu J and Luo F. CaMKII α may modulate fentanyl-induced hyperalgesia via a CeLC-PAG-RVM-spinal cord descending facilitative pain pathway in rats. *PLoS One* 2017; 12: e0177412.
 6. Guo W, Imai S, Yang JL, Zou S, Watanabe M, Chu YX, Mohammad Z, Xu H, Moudgil KD, Wei F, Dubner R and Ren K. In vivo immune interactions of multipotent stromal cells underlie their long-lasting pain-relieving effect. *Sci Rep* 2017; 7: 10107.
 7. Ni H-D, Yao M, Huang B, Xu L-S, Zheng Y, Chu Y-X, Wang H-Q, Liu M-J, Xu S-J and Li H-B. Glial activation in the periaqueductal gray promotes descending facilitation of neuropathic pain through the p38 MAPK signaling pathway. *J Neurosci Res* 2016; 94: 50–61.
 8. Roberts J, Ossipov MH and Porreca F. Glial activation in the rostroventromedial medulla promotes descending facilitation to mediate inflammatory hypersensitivity. *Eur J Neurosci* 2009; 30: 229–241.
 9. Wei F, Guo W, Zou S, Ren K and Dubner R. Supraspinal glial–neuronal interactions contribute to descending pain facilitation. *J Neurosci* 2008; 28: 10482–10495.
 10. Porreca F, Ossipov MH and Gebhart GF. Chronic pain and medullary descending facilitation. *Trends Neurosci* 2002; 25: 319–325.
 11. Gebhart GF. Descending modulation of pain. *Neurosci Biobehav Rev* 2004; 27: 729–737.
 12. Behbehani MM and Fields HL. Evidence that an excitatory connection between the periaqueductal gray and nucleus raphe magnus mediates stimulation produced analgesia. *Brain Res* 1979; 170: 85–93.
 13. Saadé NE and Jabbur SJ. Nociceptive behavior in animal models for peripheral neuropathy: spinal and supraspinal mechanisms. *Prog Neurobiol* 2008; 86: 22–47.
 14. Eidson LN and Murphy AZ. Persistent peripheral inflammation attenuates morphine-induced periaqueductal gray glial cell activation and analgesic tolerance in the male rat. *J Pain* 2013; 14: 393–404.
 15. Wan J, Ding Y, Tahir AH, Shah MK, Janyaro H, Li X, Zhong J, Vodyanoy V and Ding M. Electroacupuncture attenuates visceral hypersensitivity by inhibiting JAK2/STAT3 signaling pathway in the descending pain modulation system. *Front Neurosci* 2017; 11: 644.
 16. Ni HD, Wang Y, An K, Liu Q, Xu L, Zhu C, Deng H, He Q, Wang T, Xu M, Zheng Y, Huang B, Fang J, and Yao M. Crosstalk between nf κ b-dependent astrocytic cxcl1 and neuron cxcr2 plays a role in descending pain facilitation. *J Neuroinflammation* 2019; 16(1).
 17. Du L, Wang SJ, Cui J, He WJ and Ruan HZ. Inhibition of HCN channels within the periaqueductal gray attenuates neuropathic pain in rats. *Behav Neurosci* 2013; 127: 325–329.
 18. Du L, Wang SJ, Cui J, He WJ and Ruan HZ. The role of HCN channels within the periaqueductal gray in neuropathic pain. *Brain Res* 2013; 1500: 36–44.
 19. Wang XW, Hu S, Mao-Ying QL, Li Q, Yang CJ, Zhang H, Mi WL, Wu GC and Wang YQ. Activation of c-jun N-terminal kinase in spinal cord contributes to breast cancer induced bone pain in rats. *Mol Brain* 2012; 5: 21.
 20. Mei XP, Zhang H, Wang W, Wei YY, Zhai MZ, Wang W, Xu LX and Li YQ. Inhibition of spinal astrocytic c-Jun N-terminal kinase (JNK) activation correlates with the analgesic effects of ketamine in neuropathic pain. *J Neuroinflammation* 2011; 8: 6.
 21. Gao YJ, Xu ZZ, Liu YC, Wen YR, Decosterd I and Ji RR. The c-Jun N-terminal Kinase 1 (JNK1) in spinal astrocytes is required for the maintenance of bilateral mechanical allodynia under a persistent inflammatory pain condition. *Pain* 2010; 148: 309–319.
 22. Paxinos G WC. *The rat brain in stereotaxic coordinates*. New York: Academic Press; 1977.
 23. Keay KA, Feil K, Gordon BD, Herbert H and Bandler R. Spinal afferents to functionally distinct periaqueductal gray columns in the rat: an anterograde and retrograde tracing study. *J Comp Neurol* 1997; 385: 207–229.
 24. An K, Rong H, Ni H, Zhu C, Xu L, Liu Q, Chen Y, Zheng Y, Huang B and Yao M. Spinal PKC activation Induced neuronal HMGB1 translocation contributes to hyperalgesia in a bone cancer pain model in rats. *Exp Neurol* 2018; 303: 80–94.
 25. Urban MO and Gebhart GF. Supraspinal contributions to hyperalgesia. *Proc Natl Acad Sci U S A* 1999; 96: 7687–7692.
 26. Heinricher MM, Tavares I, Leith JL and Lumb BM. Descending control of nociception: specificity, recruitment and plasticity. *Brain Res Rev* 2009; 60: 214–225.
 27. Fields HL and Basbaum AI. Brainstem control of spinal pain-transmission neurons. *Annu Rev Physiol* 1978; 40: 217–248.
 28. Sun J, Lu B, Yao J, Lei W, Huang Y, Zhang H and Xiao C. Intra-periaqueductal gray infusion of zeta inhibitory peptide attenuates pain-conditioned place avoidance in rats. *Brain Res* 2014; 1582: 55–63.
 29. Choi H-S, Roh D-H, Yoon S-Y, Kwon S-G, Choi S-R, Kang S-Y, Moon J-Y, Han H-J, Kim H-W, Beitz A J and Lee J-H. The role of spinal interleukin-1 β and astrocyte connexin 43 in the development of mirror-image pain in an inflammatory pain model. *Exp Neurol* 2017; 287: 1–13.
 30. Sanna MD, Ghelardini C and Galeotti N. Spinal astrocytic c-Jun N-terminal kinase (JNK) activation as counteracting mechanism to the amitriptyline analgesic efficacy in painful peripheral neuropathies. *Eur J Pharmacol* 2017; 798: 85–93.
 31. Liu S, Liu YP, Lv Y, Yao JL, Yue DM, Zhang MY, Qi DY and Liu GJ. IL-18 contributes to bone cancer pain by regulating glia cells and neuron interaction. *J Pain* 2018; 19: 186–195.
 32. Luo X, Tai WL, Sun L, Pan Z, Xia Z, Chung SK and Cheung CW. Crosstalk between astrocytic CXCL12 and microglial CXCR4 contributes to the development of neuropathic pain. *Mol Pain* 2016; 12: 1–15.
 33. Tanga FY, Raghavendra V, Nutile-McMenemy N, Marks A and Deleo J A. Role of astrocytic S100 β in behavioral hypersensitivity in rodent models of neuropathic pain. *Neuroscience* 2006; 140: 1003–1010.

34. Romero-Sandoval A, Chai N, Nutile-Mcmenemy N and Deleo JA. A comparison of spinal Iba1 and GFAP expression in rodent models of acute and chronic pain. *Brain Res* 2008; 1219: 116–126.
35. Hu XF, He XT, Zhou KX, Zhang C, Zhao WJ, Zhang T, Li JL, Deng JP and Dong YL. The analgesic effects of triptolide in the bone cancer pain rats via inhibiting the upregulation of HDACs in spinal glial cells. *J Neuroinflammation* 2017; 14: 213.
36. Hang LH, Li SN, Luo H, Shu WW, Mao ZM, Chen YF, Shi LL and Shao DH. Connexin 43 mediates CXCL12 production from spinal dorsal horn to maintain bone cancer pain in rats. *Neurochem Res* 2016; 41: 1200–1208.
37. Lu C, Liu Y, Sun B, Sun Y, Hou B, Zhang Y, Ma Z and Gu X. Intrathecal injection of JWH-015 attenuates bone cancer pain via time-dependent modification of pro-inflammatory cytokines expression and astrocytes activity in spinal cord. *Inflammation* 2015; 38: 1880–1890.
38. Maoying QL, Wang XW, Yang CJ, Xiu L, Mi WL, Wu GC and Wang YQ. Robust spinal neuroinflammation mediates mechanical allodynia in Walker 256 induced bone cancer rats. *Mol Brain* 2012; 5: 16.
39. Ducourneau VRR, Dolique T, Hachem-Delaunay S, Miraucourt LS, Amadio A, Blaszczyk L, Jacquot F, Ly J, Devoize L, Olliet SHR, Dallel R, Mothet J-P, Nagy F, Fénelon VS and Voisin DL. Cancer pain is not necessarily correlated with spinal overexpression of reactive glia markers. *Pain* 2014; 155: 275–291.
40. Liu X, Bu H, Liu C, Gao F, Yang H, Tian X, Xu A, Chen Z, Cao F and Tian Y. Inhibition of glial activation in rostral ventromedial medulla attenuates mechanical allodynia in a rat model of cancer-induced bone pain. *J Huazhong Univ Sci Technol [Med Sci]* 2012; 32: 291–298.
41. Mor D, Bembrick AL, Austin PJ, Wyllie PM, Creber NJ, Denyer GS and Keay KA. Anatomically specific patterns of glial activation in the periaqueductal gray of the subpopulation of rats showing pain and disability following chronic constriction injury of the sciatic nerve. *Neuroscience* 2010; 166: 1167.
42. Mor D, Bembrick AL, Austin PJ and Keay KA. Evidence for cellular injury in the midbrain of rats following chronic constriction injury of the sciatic nerve. *J Chem Neuroanat* 2011; 41: 158–169.
43. Chu H, Sun J, Xu H, Niu Z and Xu M. Effect of periaqueductal gray melanocortin 4 receptor in pain facilitation and glial activation in rat model of chronic constriction injury. *Neurol Res* 2012; 34: 871–888.
44. Yang Y, Li H, Li TT, Luo H, Gu XY, Lü N, Ji RR and Zhang YQ. Delayed activation of spinal microglia contributes to the maintenance of bone cancer pain in female Wistar rats via P2X7 receptor and IL-18. *J Neurosci* 2015; 35: 7950–7963.
45. Wang XW, Hu S, Mao-Ying QL, Li Q, Yang CJ, Zhang H, Mi WL, Wu GC and Wang YQ. Activation of c-jun N-terminal kinase in spinal cord contributes to breast cancer induced bone pain in rats. *Mol Brain* 2012; 5: 1–7.
46. Wang C, Kong X, Zhu C, Liu C, Sun D, Xu Q, Mao Z, Qin Q, Su H, Wang D, Zhao X, and Lin N. Wu-tou decoction attenuates neuropathic pain via suppressing spinal astrocytic IL-1R1/TRAF6/JNK signaling. *Oncotarget* 2017; 8: 92864.
47. Tang J, Zhu C, Li ZH, Liu XY, Sun SK, Zhang T, Luo ZJ, Zhang H and Li WY. Inhibition of the spinal astrocytic JNK/MCP-1 pathway activation correlates with the analgesic effects of tanshinone IIA sulfonate in neuropathic pain. *J Neuroinflammation* 2015; 12: 57.
48. Zhang ZJ, Cao DL, Zhang X, Ji RR and Gao YJ. Chemokine contribution to neuropathic pain: respective induction of CXCL1 and CXCR2 in spinal cord astrocytes and neurons. *Pain* 2013; 154: 2185–2197.
49. Du JY, Fang JQ, Liang Y and Fang JF. Electroacupuncture attenuates mechanical allodynia by suppressing the spinal JNK1/2 pathway in a rat model of inflammatory pain. *Brain Res Bull* 2014; 108: 27–36.
50. Guo CH, Bai L, Wu HH, Yang J, Cai GH, Wang X, Wu SX and Ma W. The analgesic effect of rolipram is associated with the inhibition of the activation of the spinal astrocytic JNK/CCL2 pathway in bone cancer pain. *Int J Mol Med* 2016; 38: 1433–1442.
51. Gao YJ, Zhang L, Samad OA, Suter MR, Yasuhiko K, Xu ZZ, Park JY, Lind AL, Ma Q and Ji RR. JNK-induced MCP-1 production in spinal cord astrocytes contributes to central sensitization and neuropathic pain. *J Neurosci* 2009; 29: 4096–4108.